Composites Part B 170 (2019) 11–18

Contents lists available at ScienceDirect

Composites Part B

journal homepage: www.elsevier.com/locate/compositesb

Comparison of interfacial adhesion of hybrid materials of aluminum/carbon fiber reinforced epoxy composites with different surface roughness

Dong-Jun Kwon [a], Jong-Hyun Kim [b], Yu-Jeong Kim [a], Jin-Jae Kim [a], Sung-Min Park [a], Il-Jun Kwon [a], Pyeong-Su Shin [b], Lawrence K. DeVries [c], Joung-Man Park [b,c,*]

[a] Polymer Resin Team, Korea Dyeing and Finishing Technology Institute, Daegu, 41706, Republic of Korea
[b] Department of Materials Engineering and Convergence Technology, Gyeongsang National University, Jinju, 52828, Republic of Korea
[c] Department of Mechanical Engineering, The University of Utah, Salt Lake City, UT, 84112, USA

ARTICLE INFO

Keywords:
Hybrid materials
Interfacial adhesion
Lap shear strength (LSS)
Surface roughness

ABSTRACT

This study investigated the effect of surface roughness for improving interfacial adhesion in hybrid materials with aluminum (Al)/carbon fiber reinforced epoxy composites (CFREC). The surface roughness of the Al was controlled using different types of sanding paper and varied sanding times. Al surface roughness were evaluated using static contact angle (CA) and 3D surface scanning measurements after the different sanding processes. Lap shear strength (LSS) tests were performed to evaluate the interfacial adhesion between CFREC and Al with the different Al surface treatments. The theoretical maximum cohesive strength (TMCS) and work of adhesion, W_a between the Al and CFREC were correlated with surface energy of epoxy adhesive and LSS. The surface energy of epoxy adhesive and TMCS between CFREC and Al exhibited a proportional relationship. The TMCS was also directly related to the LSS between Al and CFREC. It was found that an optimum sanding process yielding a R_a, 1.4 μm Al surface roughness exhibited the highest work of adhesion, as well as the largest LSS and TMCS for hybrids of Al-CFREC. Proper Al surface control in these materials shows real promise for enhancing the mechanical properties for aerospace, automotive and other practical applications.

1. Introduction

Composite materials are currently finding greatly increased usage in a variety of fields, such as military, aerospace, rope, construction and automobile, due to their favorable mechanical properties and lightweight [1–3]. Factors that tend to limit composite usage include cost and difficult manufacturing processes that are not readily adapted to mass production. Composite-metal hybrid structure bonding methods have been proposed as a partial solution to these problems [4–6].

The bonding technique has been divided into several main methods. First, the common technique of physical and mechanical bonding methods. More recently, the self-piercing riveting (SPR) has been developed to prevent peeling damage in composites during, for example, the drilling processes [7]. These methods, being developed and under study using friction, include: stir welding (FSW) [8], friction stir blind riveting (FSBR) [9], friction stir spot joining (FSSJ) [10], mechanical clinching [11], laser assisted metal, and plastic (LAMP) [12]. Another method was to bond dual materials using structural adhesive is by chemical bonding [13–15]. Recently, several studies had been conducted on bonding methods that contribute to the reduction of noise and vibration by filling the voids between interface parts. Moreover, some of these methods may also significantly simplify the manufacturing process.

If a structural adhesive is used, it was recommended it satisfy US Federal Standard, FS-MMM-A-132B [16], and that its interfacial adhesive properties was measured by T-peel [17,18], and the lap shear strength (LSS) test [19] etc. In addition, it is essential to understand the composition of the chemical adhesive, and the adherend surface to facilitate the optimization of the chemical bonding process.

Da Silva et al. studied creep and bonding strength effects for a variety of adhesives. They experimentally demonstrated that adhesive strength depends on adhered, adhesive thickness, adhered strength and hardness the surface treatment between adherend and adhesive, curing time, surface roughness [20,21]. Kahraman used FEM simulations and experiments to evaluate the effects of adhesive thickness on bonding strength and Fracture [22]. Tezcan investigated the effect of surface

* Corresponding author. Department of Materials Engineering and Convergence Technology, Gyeongsang National University, Jinju, 52828, Republic of Korea.
E-mail address: jmpark@gnu.ac.kr (J.-M. Park).

https://doi.org/10.1016/j.compositesb.2019.04.022
Received 5 January 2019; Received in revised form 10 April 2019; Accepted 22 April 2019
Available online 23 April 2019
1359-8368/

roughness on the bonding strength under static and dynamic loading conditions and reported that there was low strength at surface roughnesses of $R_a < 0.1$ μm and $R_a > 2.5$ μm, with the maximum strength occurs between 1.5 and 2.5 μm [23,24]. It was observed that high surface roughness results in high adhesive strength by evaluating the cleavage joint strength subsequent grit blasting and diamond polishing method [25]. It was also found that an optimum value of surface roughness existed with respect to the tensile strength of the adhesion, although a relationship between peel test and surface roughness was not as obvious [26]. However, they confirmed that the cleaning of adhered surface was an important factor in bonding strength development because it affects both oil and abrasion. Based on these studies, Ghumatkar investigated optimal surface roughness values were found by studying the effect of adhered surface roughness on the adhesive bonding strength using the single strap joint test [27].

In this study, modified surface of Al was produced using different sanding processes; Specimens using these Al modifications were tested to determine the effect of surface roughness on LSS, TMCS, and work of adhesion between CFREC and the Al. In addition, static CA and 3D surface scanning measurements were used to explore how the use of different types of sanding paper and sanding times effected the surface roughness changes of the Al. Specimens of these materials were also tested to see how the surface roughness modifications effected LSS, surface energy, W_a TMCS, etc.

2. Experimental

2.1. Materials

The materials used in this study were CFREC (UD high speed cured, TB carbon Co., Ltd., Korea) and aluminum (Al-5052, Henan Xinyu nonferrous metal Co., Ltd., China). The CFRP composite was manufactured using T-700 grade carbon fiber (Toray, Japan), YD-128 epoxy (Kukdo Chemical, Korea) and dicyandiamine hardener (Adekakorea, Korea). The plate specimens of both Al and CFREC were optimized to the size of 10 mm width × 60 mm length × 2 mm thickness, which was cut by a diamond cutter (MBS 220E, Proxxon Co., LTD., Japan) to produce lap shear test specimens. A high stiffness structural adhesive (D type, Kospol Co., Ltd., Korea) was used in manufacturing the dual material specimens.

2.2. Methodologies

2.2.1. Surface roughness of Al by sanding, and 2D and 3D observation of surface conditions

The surface of Al was exposed to different sanding treatments to investigate for the difference in adhesion strength. The surface roughness was measured by using 3 types of sandpaper (p120, p220, and p400) of sandpapers (Mirka gold, Mirka Co., Ltd., U.S.A.) and for different elapsing times of sanding (30s, 60s, and 180s). A sanding machine (Mirka ROS625CV, Mirka Co., Ltd., U.S.A.) was performed at 12,000 RPM, with air pressure of 5 kg/cm^2. After sanding process, acetone was used to remove remaining residual particles on the Al surface, followed by drying at 40 °C for one day. The 2D surfaces of the Al were observed using a USB type microscope (AM7013MT, Dino lite Co., Ltd., Taiwan). A 3D optical surface profiler (NV-2700, Nanosystems Co., Ltd., Korea) was used to observe the 3D nature of the Al and to measure the roughness of the Al. Changes in R_a of the Al surface roughness, as a function of the different sanding treatments, were recorded. In addition, the contact angle (CA) of Al was measured using distilled water for the different conditions of surface roughness. To facilitate these CA measurements a uniform water droplet with 1 mm diameter was placed on the Al surfaces of different roughness with a syringe pump.

Table 1
The correlation of surface energy of adhesive and TMCS of CFRP-Al hybrid materials different curing time.

	Curing time (Min)	γ_s (mJ/m^2)	γ_s^{LW} (mJ/m^2)	γ_s^{AB} (mJ/m^2)	γ_s^+ (mJ/m^2)	γ_s^- (mJ/m^2)	γ^d (mJ/m^2)	γ^p (mJ/m^2)	W_a of between D type and Al (mJ/m^2)	TMCS[a] of D type (GPa)
Al 5052	–	42.5	42.0	0.5	4.0	0.0	36.5	2.3	–	–
D type	20	50.1	40.1	9.8	15.0	1.6	26.3	4.5	87.1	6.1
	25	41.7	40.6	6.1	0.4	0.7	22.9	2.1	85.9	5.5
	30	32.6	28.6	5.1	6.4	1.0	17.9	1.5	73.3	4.9
	40	29.1	24.2	4.2	6.1	0.8	15.0	1.2	67.3	4.6

[a] TMCS: Theoretical maximum cohesive strength.

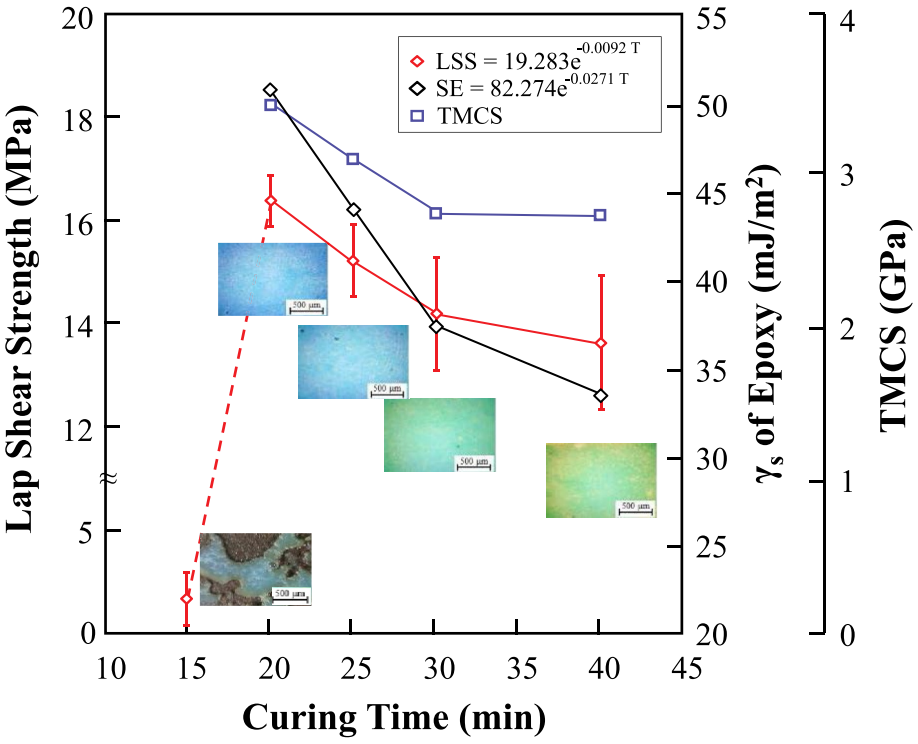

(a)

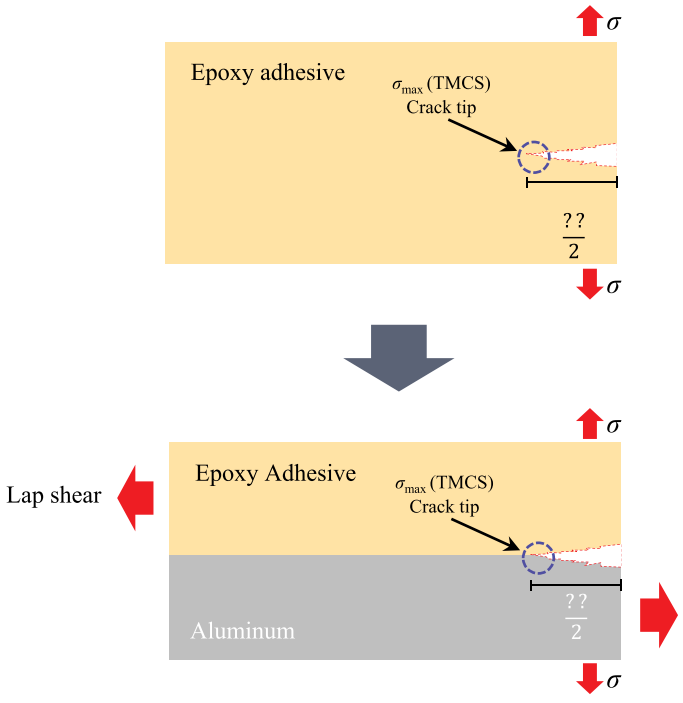

(b)

Fig. 1. (a) Correlation between LSS, surface energy, and TMCS of CFRP-Al hybrid material and actual surface of cured epoxy adhesive over time; and (b) schematic modeling of fracture mechanism for single and multi-materials.

2.2.2. Lap shear test of dual materials of CFREC/Al with different sanding conditions

A universal testing machine (UTM) (AGS- X0K, Shimadzu Co., Ltd., Japan) was used for the lap shear test. The sub-sized specimens were prepared based on ASTM D5868. Seven experiments were carried out using Al with different surface roughness specimens. The data were obtained by averaging the results of 7 tests, except for the maximum and minimum values. Lap shear strength (LSS) between CFREC and Al were

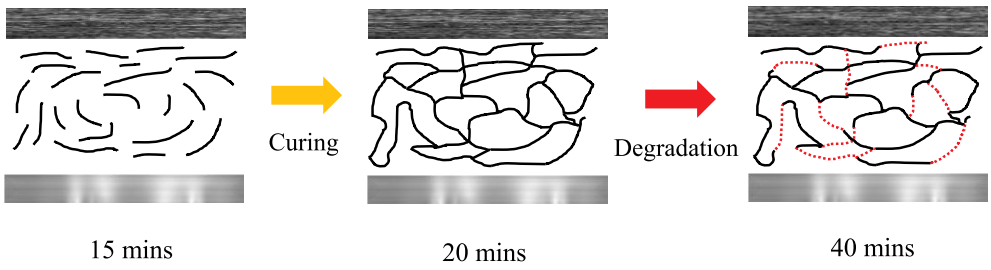

Fig. 2. Schematic modeling of the interface with curing and degradation.

evaluated using the following equation:

$$\text{Lap Shear strength (LSS)} = \frac{F}{A_a} \tag{1}$$

where F is the failure force of the specimen, and A_a is the 'adhesive area' of between CFREC and Al [28].

2.2.3. Evaluation of CA, work of adhesion, W_a and TMCS of the dual materials, for different Al surface conditions

The CA measurements are generally used to analyze the surface energy of Al and adhesive materials. In this study, the static CA measurement was used to evaluate the surface energy of Al with different roughness using four different kinds of solvents (i.e., distilled water, formamide, ethylene glycol and diiodomethane) on the Al surfaces.

The total surface energy, γ^T, is the sum of the Lifshitz-van der Waals component, γ^{LW} and acid-base component, γ^{AB}. The calculation of the above components, following the modified young-Dupre equation of the work of adhesion, W_a can be expressed as [29]:

$$W_a = \gamma_L(1+\cos\theta) = 2\left(\gamma_L^{LW}\gamma_S^{LW}\right)^{\frac{1}{2}} + 2\left[\left(\gamma_S^-\gamma_L^+\right)^{\frac{1}{2}} + \left(\gamma_S^+\gamma_L^-\right)^{\frac{1}{2}}\right] \tag{2}$$

A common approach in considering solid surface energy is to express them as a sum of dispersive and polar components, which can affect the work of adhesion, W_a, between the structural adhesive and the Al substrate. The work of adhesion between the adhesive material and Al was determined to provide insight and knowledge of the interfacial adhesion.

The TMCS formula was used to predict the adhesive strength between different materials using surface energy, which can be expressed as [30]:

$$\sigma_m = \left(\frac{2E\gamma}{\pi a}\right)^{\frac{1}{2}} \tag{3}$$

Where σ_m is the theoretical maximum cohesive strength, E is Young's modulus of epoxy adhesive, a is a crack length, γ is the surface energy of adhesive. This empirical formula was derived by analyzing the correlation using the TMCS, work of adhesion, interfacial adhesion, solid surface energy and LSS. TMCS of epoxy adhesive was obtained using equation (3) with E, 7.3 GPa, Poisson's ratio, 0.4, and a,1 cm.

3. Results and discussion

3.1. Correlation among LSS, TMCS and surface energy

Table 1 summarizes the determined surface energies for the epoxy adhesives with different curing times as well as W_a and TMCS of these epoxy adhesives determined from the static contact angle measurements along with equations (2) and (3). The values of $\boldsymbol{\gamma^p}$ and $\boldsymbol{\gamma_s}$ for epoxy adhesive decreased with increasing curing time comparing to those with twenty minutes curing. Even after the curing state of the epoxy adhesive exceeds over 100%, the values of $\boldsymbol{\gamma^p}$ and $\boldsymbol{\gamma_s}$ decrease because the reactivity of epoxy adhesive decreases as the aging time increases at such a high 180 °C. The work of adhesion between Al and the epoxy adhesive, W_a, decreased as the surface energy of the epoxy adhesive decreased. The higher the surface energy of epoxy adhesive, the higher the work of adhesion between the dual materials. This can be also because the surface energy of the epoxy adhesive decreases as the curing time increases. TMCS exhibited that the cohesion strength of epoxy adhesive at the interface decreases with increasing curing time due to decreased self-cohesion of the epoxy adhesives. It may be because TMCS indicates the degree of cohesion of the epoxy adhesive unlike W_a. As the curing time of epoxy adhesive increased, the bond strength between the internal polymer chains of epoxy adhesive improves [31,32]. As the curing time increases, the active functional groups present on the surface of the epoxy adhesive decreases and thus the surface energy decreases. TMCS can be used to approximate the level of self-adhesion of the epoxy adhesive themselves, whereas the work of adhesion at interface can be analyzed using W_a. TMCS involves the surface energy of only the adhesive, whereas W_a entails the surface energy between the adhesive and the matrix. Nonetheless, W_a and TMCS exhibited a proportional relationship, as demonstrated in Table 1 and Fig. 1.

Fig. 1(a) and Table 1 show LSS, TMCS and surface energy for epoxy adhesive for the dual material as functions of curing time. The adhesive strength (e.g. the LSS) decreased with different curing times. Apparently the adhesive was not cured well until 15 min curing time (at which time the LSS was approximately 3 MPa). Clearly sufficient time was needed for the composition of the epoxy adhesive to change from a gel to a more solid state. At 15 min cure time the solidification by curing had started to occur and thus interfacial epoxy adhesion between Al and CFREC could be formed. The maximum LSS was observed to occur at 20 min curing time. As expected, the adhesion strength increased as the curing time increased. As shown in Fig. 1(a), some discoloration occurred during curing, which was attributed to the relatively high 180 °C curing temperature. The surface energy of the adhesive also decreased with increasing curing time due to deteriorated epoxy adhesive due to the longer exposure to the high 180 °C temperature.

Fig. 1(b) shows the schematic modeling of the fracture mechanism for single (TMCS) and dual-materials (interfacial adhesion as ILL) based on equation (3). The TMCS can be used to predict the cohesive strength between identical two materials. Since TMCS also exhibited a similar trend with LSS and surface energy of epoxy adhesive, thermodynamical surface energy and practical mechanical LSS should be consistent with each other. Fig. 2 shows schematic plots of the change in morphology at the interface during the curing process of the epoxy adhesive with increasing cure time. These sketches exhibit pre-curing, optimal curing and then the degraded condition associated with over-curing. This latter state can be related to a reduction in LSS, surface energy and TMCS. In summary epoxy adhesive can need an optimum curing time. In case they have a curing time longer than the optimum time, the epoxy adhesive can undergo thermal aging in the cured states. It resulted in the reduction of adhesion between dual materials due to decreased surface energy. It could be expected that the adhesion between the dual materials could be comparatively predicted by calculating TMCS if the surface energy of the adhesive could be obtained.

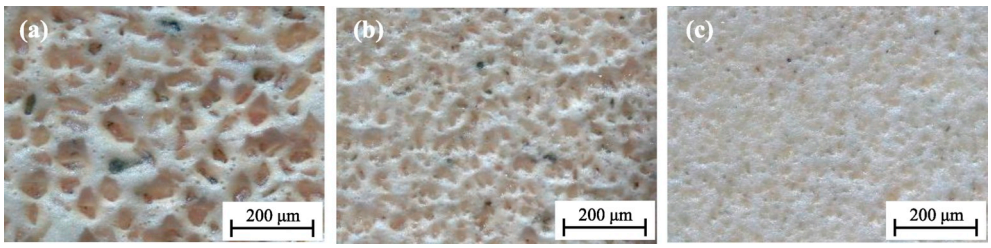

Fig. 3. Photos of surface of sandpaper: (a) p120; (b) p220; and (c) p400 surfaces.

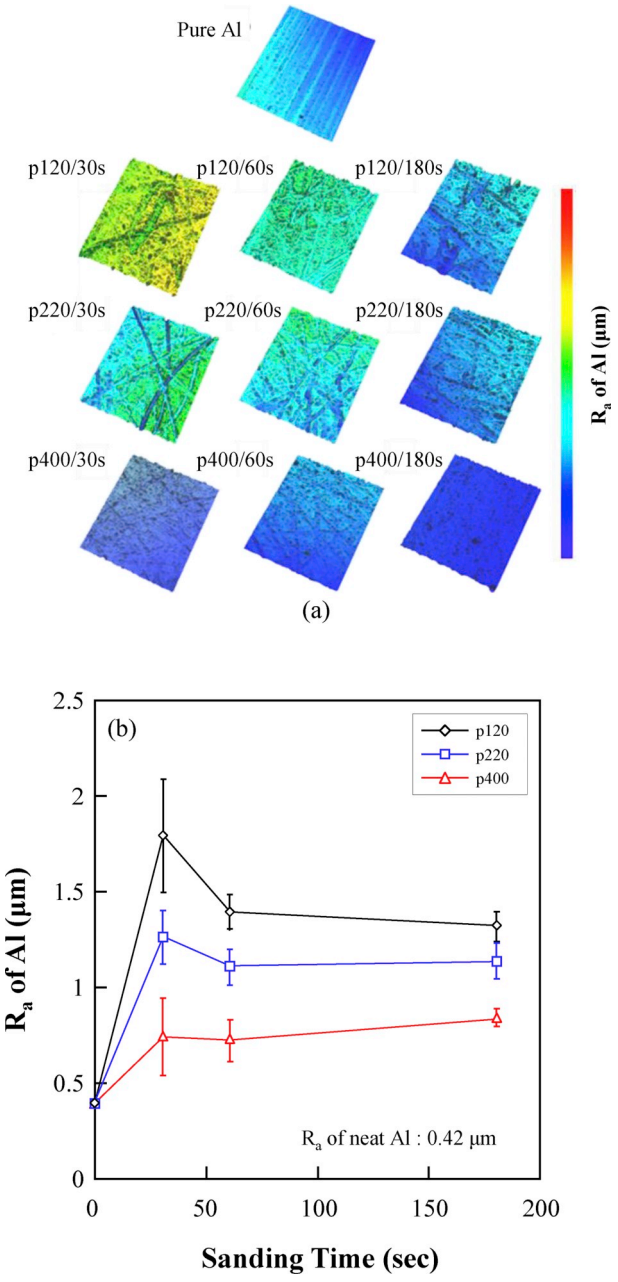

Fig. 4. (a) Photos of R_a of Al surface with different sanding processes; and (b) R_a of Al surface with different sanding time.

3.2. Effect of Al roughness of Al on adhesion of dual materials

Fig. 3 exhibits optical microscope photos of the surface of the different sandpapers used in this study (note, the higher the sandpaper's p-number the lower the sandpaper roughness). Fig. 4(a) shows the surface R_a obtained using a 3D optical surface profiler machine for different sanding conditions. This 3D profiler was to scan the samples in each of the X, Y, and Z directions by using a 3D profiler. The R_a scanning in the Z direction of surface yields the average roughness value of the surface. The parameters representing the state of roughness are displayed in various forms. The value of 'Arithmetical mean height being the mean surface roughness' indicated by S_a (in ISO 25178-2, 2012) was used as R_a in the equipment in this work [33]. As sanding time increased, more uniform surfaces could be formed. In case p120, rough surface can be formed in a short time, whereas in p400 case surface roughness did not change in either short or long sanding time.

Fig. 4(b) shows R_a of Al resulting from different sanding conditions based on Fig. 4(a). R_a increases rather rapidly in the first 30 s of sanding, for all three sand papers, followed by decreases in R_a for two sandpapers while it remains relatively constant for the fine sand paper during the next 30 s and R_a changes only slightly for the next 120 s for all three sandpapers. In case P120, surface roughness, R_a increased approximately 4 times more compared to neat Al case, 0.42 μm. However, after 180 s sanding time, R_a became more uniform state as R_a to be 1.4 μm. In p220 like 120 cases, with increasing sanding time R_a increased with 30 s sanding time, and then decreased with increasing further. In the p440 case R_a exhibits the rather reduced increment after sanding for 30 s, however, it continued to increase gradually.

Fig. 5 shows the static CA results for specimens sanded with the three different sand papers versus sanding time surface treatments. Before sanding the Al specimens exhibited a CA of just under 95°. The CA changed dramatically with sanding treatment for the P120 sandpaper, the CA remained relatively constant during the first 30 s of sanding rapidly dropped to below 60° in the next 30 s and then remained relatively constant in the next 120 s. For the p220 sandpaper, the CA increased initially to over 100° at 30 s sanding time after which it steadily decreased to near 75° at 180 s sanding time. The p400 sandpaper behaved distinctly differently, after an increase of 2 or 3 degrees in the first 30 s of sanding time its CA remained relatively constant at about 95° to 180 s.

The surface roughness of Al was also changed significantly with increasing sanding time and comparing the surfaces suggests that the P120 sandpaper is optimal.

Fig. 6 shows the LSS for dual material specimens using structural epoxy adhesives between CFREC and Al with different surface roughness, and their surface energy of Al and LSS. The shorter the sanding treatment time, the lower the LSS and the lower the surface energy. While the effect of surface roughness is important, too short of sanding time exhibited he larger R_a deviation as shown in Fig. 4. Since the short sanding treatments did produce a uniform surface, resulting in a lowered adhesive force. Fig. 6(a), shows that there is a minimal effect on when the sandpaper producing the lower roughness was used. Use of the rough sandpaper and increased sanding times resulted in higher adhesion between CFREC and Al as well as a more stable and uniform R_a. Fig. 6(b) shows that there is an approximately proportional relationship between the LSS and the surface energy of epoxy adhesive. The higher the surface energy, the larger the LSS.

Based on the experimental outcomes of Figs. 4–6, two important

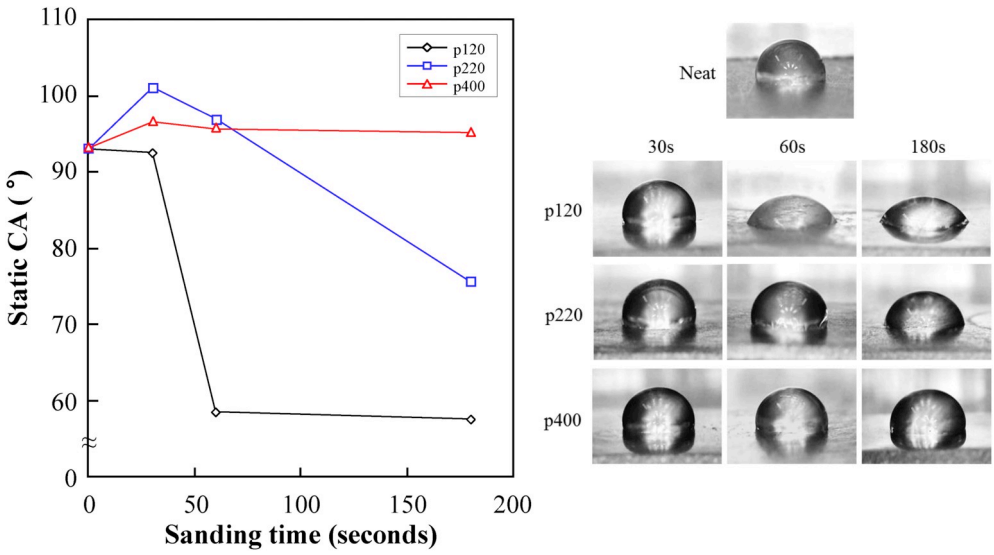

Fig. 5. Static CA of Al surface with different sanding time.

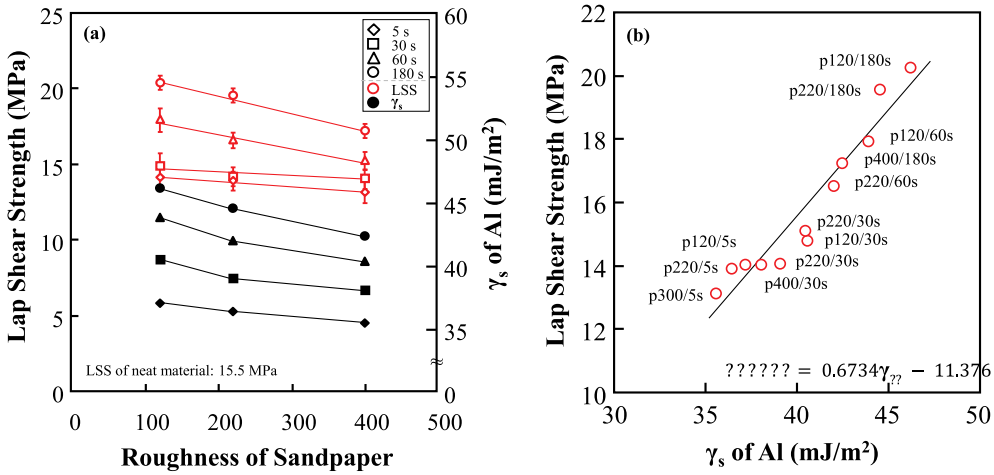

Fig. 6. LSS of CFRP-Al hybrid materials and surface energy of Al with different sanding processes: (a) the correlation between LSS and γ_s with different sanding condition; and (b) empirical formula form γ_s *versus* LSS (Average of LSS of CFRP/Al γ_s of pure Al: 42.5 mJ/m^2).

factors were identified. First, if the sanding process was performed within 30 s regardless of the type of sandpaper, the roughness level increased sharply compared to the surface roughness of the initial material. However, the adhesion was not enhanced stably because of the uneven surface roughness. Second, if the sanding time was set as one minute or more depending on the type of sandpapers, the surface roughness becomes uniform. It is also possible to identify the optimum R_a of surface for reinforcing the adhesive strength between dual materials *via* a variety of other experiments. However, it could be concluded from this study that the state having R_a of 1.4 μm with uniform surface was the optimum surface roughness of Al for reinforcing the adhesive strength.

Fig. 7 shows the work of adhesion, W_a between Al and the epoxy adhesive and LLS for the different sandpapers used to produce surface roughness *versus* sanding time. The W_a initially decreased and then increased which is attributed to the longer sanding times, producing non-uniform-rough surfaces which prevents good bonding. The increased adhesion, exhibited after 30 s sanding is considered to be due to more uniformly rough surfaces. W_a and LSS exhibited similar trends with sanding time. Ultimately, appropriate sanding treatments were effective for improving adhesion in the dual materials specimens. It was important to obtain the optimum physical surface roughness because adhesion depends on the R_a of the surface as well as the chemical composition of the materials. The most improved adhesion was obtained by using the rougher sandpaper, P120, for at least 1 min.

Fig. 8 exhibits schematic modeling of three patterns of the interfacial conditions for three different sanding processes. As expected, the surface roughness of Al increased with increased sanding time. The interfacial adhesion between sanded Al and epoxy adhesive increased over that of a neat Al specimen. Controlling the roughness of the matrix using sandpaper was found to be an important parameter affecting on adhesion between dual materials. From the sanding process for more than one minute, the surface roughness of the Al matrix exhibited a specific R_a value with the different composition of the sandpapers. It could be expected that the adhesion strength can be enhanced by obtaining the optimum R_a between dual materials.

4. Conclusions

A goal of this work was to improve the interfacial adhesion between an epoxy and Al by varying the surface roughness of the Al. The surface roughness of the Al was controlled by using different types of sandpapers and varying the sanding time. The R_a decreased steeply in the first 60 s of sanding and then increased. Static CA and work of adhesion, W_a also

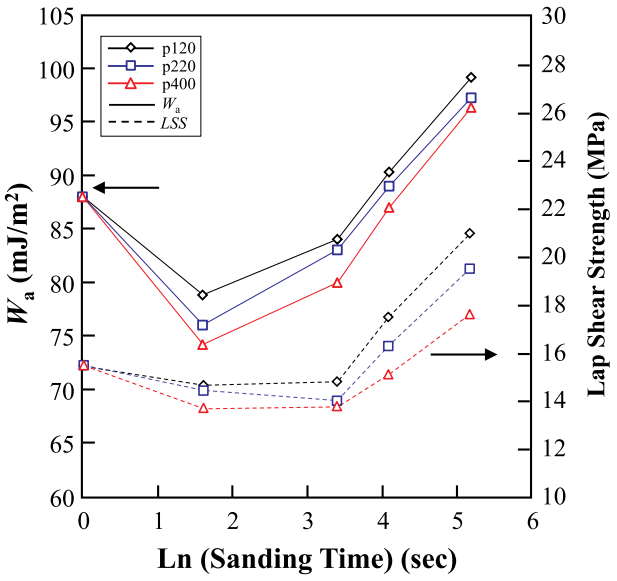

Fig. 7. W_a of CFRP-Al hybrid materials with different sanding (Surface energy of CFRP: 46.5 mJ/m^2, W_a between CFRP and Adhesion: 84.9 mJ/m^2).

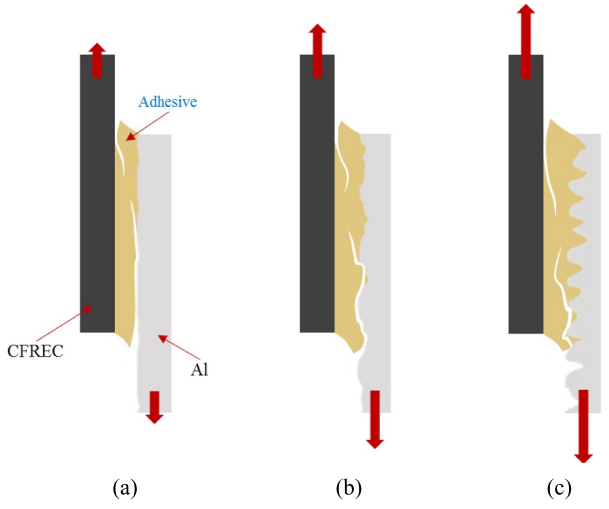

Fig. 8. Schematic modeling of the interface using different roughness typed Al with different sanding times: (a) 30; (b) 60; and (c) 180 s.

changed with different surface roughness. Static CA increased up to 30 s of sanding time and then decreased which was possibly related to the uniformity of the roughness. The change in surface energy of epoxy adhesive with curing time was consistent with the measured TMCS and the LSS of the dual specimens. The suitable surface roughness of Al can contribute to optimal mechanical interlocking and associated properties. In this study, P 120 sand paper with longer sanding time, resulted in both high W_a and LSS. This is attributed to the longer sanding times resulting in increased surface energy of Al with an associated improved W_a between Al and epoxy adhesive. Furthermore, the increased surface energy results in improved mechanical adhesion. Properly-controlled roughness of the Al surface combined with maximized LSS associated with favorable CA, Al surface energy, as well as optimized curing and TMCS of epoxy adhesive all contributed to the maximum LSS.

Acknowledgements

This work was supported by Korea Evaluation Institute of Industrial Technology and Ministry of Trade, Industry and Energy under the contract No. 10063368, 2016–2020.

References

[1] US army research laboratory. Compos Mater Handb 2002;3.
[2] Karthigeyan P, Raja MS, Hariharan R, Karthikeyan R, Prakash S. Performance evaluation of composite material for aircraft industries. Mater Today: Proceedings 2017;4:3263–9.
[3] Ishikawa T, Amaoka K, Masubuchi Y, Yamamoto T, Yamanaka A, Arai M, Takahashi J. Overview of automotive structural composites technology developments in Japan. Compos Sci Technol 2018;155:221–46.
[4] Camanho PP, Fink A, Obst A, Pimenta S. Hybrid titanium–CFRP laminates for high-performance bolted joints. Compos Appl Sci Manuf 2009;40:1826–37.
[5] Kashaev N, Ventzke V, Riekehr S, Dorn F, Horstmann M. Assessment of alternative joining techniques for Ti–6Al–4V/CFRP hybrid joints regarding tensile and fatigue strength. Mater Des 2015;81:73–81.
[6] Hamil L, Nutt S. Adhesion of metallic glass and epoxy in composite-metal bonding. Compos B Eng 2018;134:186–92.
[7] Gay A, Lefebvre F, Bergamo S, Valiorgue F, Chalandon P, Michel P, Bertrand P. Fatigue performance of a self-piercing rivet joint between aluminum and glass fiber reinforced thermoplastic composite. Int J Fatigue 2016;83:127–34.
[8] Avettand-Fenoel MN, Simar A. A review about Friction Stir Welding of metal matrix composites. Mater Char 2016;120:1–17.
[9] Lathabai S, Tyagi V, Ritchie D, Kearney T, Finnin B. Friction stir blind riveting: a novel joining process for automotive light alloys. SAE Int J Mater Manuf 2011;4:589–601.
[10] Boldsaikhan E, Fukada S, Fujimoto M, Kamimuki K, Okada H, Duncan B, Bui P, Yeshiambel M, Brown B, Handyside A. Refill friction stir spot joining for aerospace aluminum alloys. Frict Stir Weld Process 2017;IX:237–46.
[11] Lambiase F, Ko DC. Two-steps clinching of aluminum and carbon fiber reinforced polymer sheets. Compos Struct 2017;164:180–8.
[12] Roesner A, Scheik S, Olowinsky A, Gillner A, Reisgen U, Schleser M. Laser assisted joining of plastic metal hybrids. Phys Procedia 2011;12:370–7.
[13] Subramanian RV. Chemistry of adhesion. Chem Solid Wood 1984;207:323–48.
[14] Pantelakis S, Tserpes KI. Adhesive bonding of composite aircraft structures: challenges and recent developments. Sci China Phys Mech Astron 2014;57:2–11.
[15] Budhe S, Banea MD, de Barros S, da Silva LFM. An updated review of adhesively bonded joints in composite materials. Int J Adhesion Adhes 2017;72:30–42.
[16] FS-MMM-A-132B: federal specification: adhesives, heat resistant, airframe structural, metal to metal.
[17] Mi Z, Liu Z, Yao J, Wang C, Zhou C, Wang D, Zhao X, Zhou H, Zhang Y, Chen C. Transparent and soluble polyimide films from 1,4:3,6-dianhydro-D-mannitol based dianhydride and diamines containing aromatic and semiaromatic units: preparation, characterization, thermal and mechanical properties. Polym Degrad Stabil 2018;151:80–9.
[18] Teixeira de Freitas S, Banea MD, Budhe S, de Barros S. Interface adhesion assessment of composite-to-metal bonded joints under salt spray conditions using peel tests. Compos Struct 2017;164:68–75.
[19] Khali SMR, Shokuhfar A, Hoseini SD, Bidkhori M, Khalili S, Mittal RK. Experimental study of the influence of adhesive reinforcement in lap joints for composite structures subjected to mechanical loads. Int J Adhesion Adhes 2008;28:436–44.
[20] Marques EAS, Carbas RJC, Silva F, da Silva LFM, de Paiva DPS, Magalhaes FD. Use of master curves based on time-temperature superposition to predict creep failure of aluminium-glass adhesive joints. Int J Adhesion Adhes 2017;74:144–54.
[21] da Silva LFM, Carbas RJC, Critchlow GW, Figueiredo MAV, Brown K. Effect of material, geometry, surface treatment and environment on the shear strength of single lap joints. Int J Adhesion Adhes 2009;29:621–32.
[22] Kahraman R, Sunar M, Yilbas Bekir. Influence of adhesive thickness and filler content on the mechanical performance of aluminum single-lap joints bonded with aluminum powder filled epoxy adhesive. J Mater Process Technol 2008;205:183–9.
[23] Sekercioglu T, Rende H, Gulsoz A, Meran C. The effects of surface roughness on the strength of adhesively bonded cylindrical components. J Mater Process Technol 2003;142:82–6.
[24] Sekercioglu T, Meran C. The effects of adherend on the strength of adhesively bonded cylindrical components. Mater Des 2004;25:171–5.
[25] Shahid M, Hashim SA. Effect of surface roughness on the strength of cleavage joints. Int J Adhesion Adhes 2002;22:235–44.
[26] Uehara K, Sakurai M. Bonding strength of adhesives and surface roughness of joined parts. J Mater Process Technol 2002;127:178–81.
[27] Ghumatkar A, Sekhar R, Budhe S. Experimental study on different adherend surface roughness on the adhesive bond strength. Mater Today: Proceedings 2017;4:7801–9.
[28] Shin PS, Kwon DJ, Kim JH, Lee SI, DeVries KL, Park JM. Interfacial properties and water resistance of epoxy and CNT-epoxy adhesion on GFRP composites. Compos Sci Technol 2017;142:98–106.
[29] Shin PS, Baek YM, Kim JH, Park HS, Kwon DJ, Lee JH, Kim MY, DeVries KL, Park JM. Interfacial and wetting properties between glass fiber and epoxy resins with different pot lifes. Colloids Surf, A 2018;544:68–77.
[30] Sørensen BF. Cohesive law and notch sensitivity of adhesive joints. Acta Mater 2002;50:1053–61.

[31] Amariutei OA, Capper RR, Álvarez MC, Chan LKY, Foreman JP. Modelling the properties of a difunctional epoxy resin cured with aromatic diamine isomers. Polymer 2018;156:203–13.

[32] Genty S, Tingaut P, Aufray M. Fast polymerization at low temperature of an infrared radiation cured epoxy-amine adhesive. Thermochim Acta 2018;666:27–35.

[33] Ţălu Ş. Micro and nanoscale characterization of three dimensional surfaces. Basics and applications. Cluj-Napoca, Romania: Napoca Star Publishing house; 2015.